OPEN

Correspondence and
requests for materials
should be addressed to
D.P.T. (dianping.
tang@fzu.edu.cn)

Enhanced Colorimetric Immunoassay Accompanying with Enzyme Cascade Amplification Strategy for Ultrasensitive Detection of Low-Abundance Protein

Zhuangqiang Gao, Li Hou, Mingdi Xu & Dianping Tang

Ministry of Education Key Laboratory of Analysis and Detection for Food Safety, Fujian Provincial Key Laboratory of Analysis and Detection for Food Safety, Department of Chemistry, Fuzhou University, Fuzhou 350108, P.R. China.

Methods based on enzyme labels have been developed for colorimetric immunoassays, but most involve poor sensitivity and are unsuitable for routine use. Herein, we design an enhanced colorimetric immunoassay for prostate-specific antigen (PSA) coupling with an enzyme-cascade-amplification strategy (ECAS-CIA). In the presence of target PSA, the labeled alkaline phosphatase on secondary antibody catalyzes the formation of palladium nanostructures, which catalyze 3,3′,5,5′-tetramethylbenzidine-H_2O_2 system to produce the colored products, thus resulting in the signal cascade amplification. Results indicated that the ECAS-CIA presents good responses toward PSA, and allows detection of PSA at a concentration as low as 0.05 ng mL^{-1}. Intra- and inter-assay coefficients of variation are below 9.5% and 10.7%, respectively. Additionally, the methodology is validated for analysis of clinical serum specimens with consistent results obtained by PSA ELISA kit. Importantly, the ECAS-CIA opens a new horizon for protein diagnostics and biosecurity.

T he important role of disease-related protein detection in the fields of biological studies, clinical diagnostics, and medical treatment has driven the ever-increasing demand for developing simple, sensitive, highly selective, and cost-effective bioassays[1–5]. Immunoassay is considered as one of the most widely used techniques for protein detection due to its high sensitivity, high specificity, excellent accuracy, and practicality[6,7]. Up to date, various methods and strategies based on different signal-transducer principles have been reported and developed for this purpose, e.g. by using surface plasmon resonance, quartz crystal microbalance, electrochemiluminescence, fluorescence (FL), chemiluminescence (CL), electrochemistry and colorimetric method[8–14]. Typically, the colorimetric method is the most commonly used method in immunoassays because of several important advantages, e.g. simplicity, practicality, low cost, and rapid/direct readout with the naked eye[6,14]. Compared with commercialized ELISA kits and CL/FL-based immunoassays, unfortunately, the majority of the currently developed colorimetric immunoassays usually involve poor sensitivity because of using the vulnerable/limited signal amplification strategies[14,15]. In contrast, the increasing demand for screening diseases at the early stage of development calls for ultrasensitive detection of biologically relevant species at an extremely low level of expression[16]. To keep pace with expectations in clinical immunoassays, there is still the quest for more flexible, yet highly sensitive, quantitative, and easy-to-use methods.

Recently, ongoing efforts have been devoted for the development of enzyme-based colorimetric immunoassays by using native enzyme labels as the signal amplification strategies, e.g. horseradish peroxidase (HRP), alkaline phosphatase (ALP) and β-galactosidase, due to their high catalytic activity, high specificity, mild reaction conditions, and easy conjugation to antibodies[17–19]. Moreover, a single enzyme molecule can also catalytically transform many molecules of substrate into a product[15]. In the conventional enzyme-based colorimetric immunoassays, unfavorably, there is for steric reasons usually a ratio of 1 : 1 for enzyme and detection antibody used. To further increase the sensitivity of enzyme-based colorimetric immunoassays, a key point is to enhance the ratio between enzyme molecule and target analyte. By and large, there are two basic schemes for this purpose. The first classical approach is to utilize the molecular biology techniques, e.g. by using polymerized enzymes, enzyme-anti-enzyme complexes, liposome-entrapped enzymes, and the biotin-avidin conjugate chemistry[20,21]. This approach usually needs multiple labels or multi-enzyme labels, thus relatively complicated and time-consuming. Another
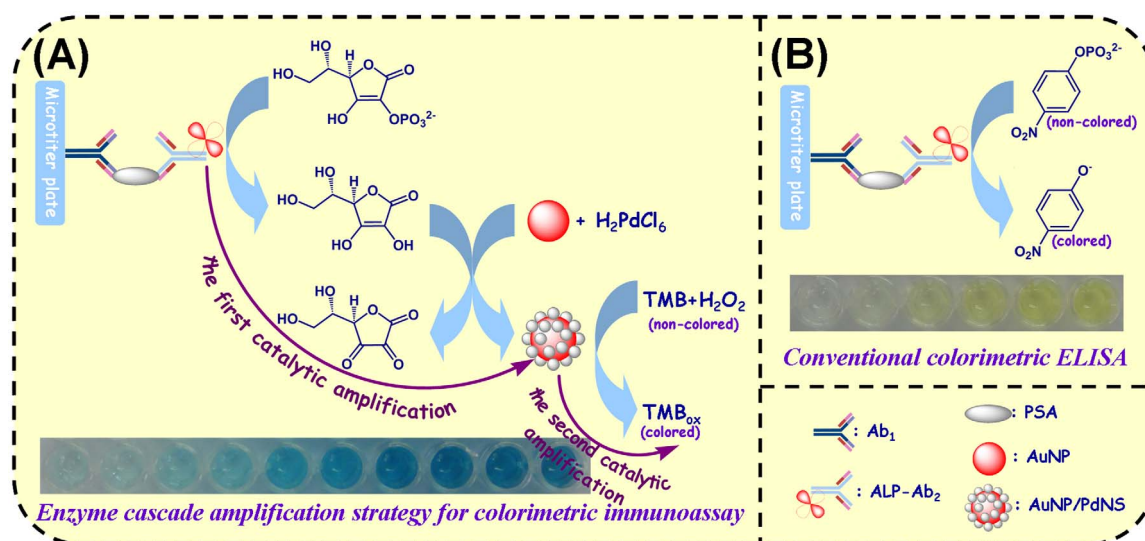
Figure 1 | Schematic illustration of (A) enhanced colorimetric immunoassay based on enzyme cascade amplification strategy (ECAS-CIA) and (B) conventional colorimetric enzyme-linked immunosorbent assay (ELISA).

approach is to employ nanomaterials as the carriers of enzymes and detection antibodies[14,17,22,23]. Zhang and co-workers designed a new ELISA strategy for highly sensitive colorimetric detection of HSP70 by using graphene nanosheets and gold nanoparticles as the carriers of HRP and antibody[17]. Compared with commercialized enzyme-labeled antibody, introduction of nanomaterial might act as a solid-phase interface for the immobilization of biomolecules. Usually, the binding capacity of the immobilized biomolecules on the solid-phase surface is less than that of soluble phase[24–26]. One major reason for the reduction of binding activity is because of steric-hindrance effect of the biomolecules in the solid phase compared with that in solution[24,25]. Another possible reason is attributed to the random orientation of the antibodies on the solid-phase surface[24,26].

Recent research has looked to develop innovative and powerful novel molecular biology methods by coupling with highly efficient nanocatalytic techniques, controlling and tailoring their properties in a very predictable manner to meet the needs of specific applications[27–30]. Enzyme cascade amplification, as a classical molecular biological technique, is extensively used for signal transduction and amplification in living system[31]. The most interesting characteristic for the enzyme cascade amplification lies in its signal amplification mechanism: an enzyme associated with a signal receptor is activated and, in turn, catalyzes the activation of many molecules of a second enzyme, each of which activates many molecules of a third enzyme, and so on[31]. Such a cascade reaction can result in the signal amplification on several orders of magnitude within milliseconds. We reasoned that if such systems could be extended to detect species other than the intracellular reaction, it might be generally useful for other types of highly sensitive and selective assays. Zuchner et al. developed a simple protease fluorescence resonance energy transfer for highly sensitive and rapid detection of enteropeptidase based on dual-enzyme cascade amplification[32]. To the best of our knowledge, there is no report focusing on enzyme cascade amplification strategy for the development of colorimetric immunoassay until now. Inspired by these advantages, our motivation in this work is to exploit an enhanced colorimetric immunoassay protocol for the detection of low-abundance proteins by coupling with enzyme cascade amplification strategy.

Prostate-specific antigen (PSA), also known as gamma-seminoprotein or kallikrein-3 (KLK3), is a glycoprotein enzyme encoded in humans by the KLK3 gene[33]. PSA is present in small quantities in the serum of men with healthy prostates, but is often elevated in the presence of prostate cancer or other prostate disorders[34,35]. As a demonstration of the capability of our design, we herein used PSA as a model analyte for the development of enhanced colorimetric immunoassay based on enzyme cascade amplification strategy. The assay is performed in a commercialized polystyrene microtiter plate conjugated with anti-PSA capture antibody, by using ALP-labeled detection antibody with a sandwich-type immunoassay format. The enzyme cascade amplification strategy is implemented by the labeled ALP to catalyze the formation of peroxidase mimics, palladium nanostructures (PdNS). And the produced PdNS can exhibit high activity to catalyze TMB-H_2O_2 system to produce colored products. By monitoring the change in the visible color or absorbance, we can qualitatively or quantitatively determine the concentration of target PSA in the sample.

Results

Construction and characteristics of the ECAS-CIA. Fig. 1A presents the assay principle of the enhanced colorimetric immunoassay based on enzyme cascade amplification strategy (ECAS-CIA). In this work, monoclonal mouse anti-human PSA antibody (Ab_1) immobilized on the surface of microtiter plates is utilized as the capture probe for target PSA, and polyclonal goat anti-human PSA antibody conjugated with alkaline phosphatase (ALP-Ab_2) is employed as detection antibody for the development of enzyme cascade amplification strategy (ECAS). The signal is amplified by the produced PdNS toward catalytic oxidation of TMB-H_2O_2 system with the aid of the labeled ALP. Fig. 2A gives the schematic illustration of ECAS triggered by the ALP. Initially, the ALP-biocatalyzed hydrolysis of ascorbic acid 2-phosphate (AA-P) leads to the formation of ascorbic acid (AA) that acts as a reducing agent for the catalytic generation of palladium nanostructures on the surface of gold nanoparticle, thus achieving the first catalytic amplification [Note: gold nanoparticles (AuNP) in this work are only used as the seeds for the growth of palladium nanostructures, and the similar protocol was also largely reported][36–38]. Then the generated PdNS can be utilized as the highly efficient peroxidase mimics to catalyze the H_2O_2-mediated oxidation of TMB to produce the colored products, thereby resulting in the second catalytic amplification[39]. Based on the designed protocol, the dual-amplification strategy can cause the cascade amplification of the detectable signal. Similar with intracellular enzyme cascade amplification strategy, the ALP-catalyzed production of PdNS-based peroxidase mimics can promote the amplification of detectable signal. In the typical PSA sandwich-type
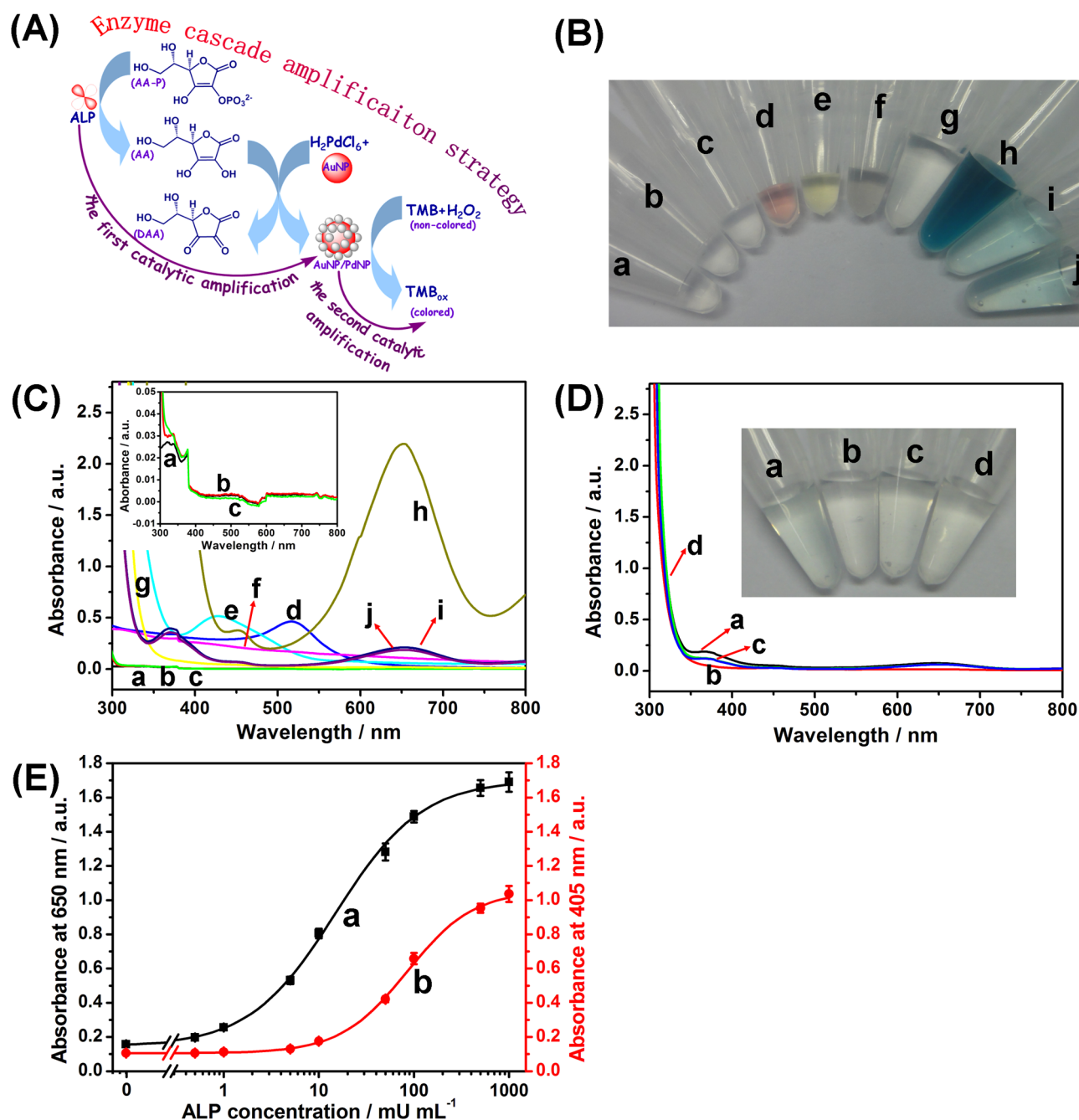
Figure 2 | (A) Schematic illustration of enzyme cascade amplification strategy (ECAS). (B) The photographs of (a) ALP, (b) AA-P, (c) ALP + AA-P, (d) AuNP, (e) K_2PdCl_6 + HCl, (f) (ALP + AA-P) + AuNP + (K_2PdCl_6 + HCl), (g) TMB + H_2O_2, (h) (ALP + AA-P) + AuNP + (K_2PdCl_6 + HCl) + (TMB + H_2O_2), (i) AA-P + AuNP + (K_2PdCl_6 + HCl) + (TMB + H_2O_2), and (j) ALP + AuNP + (K_2PdCl_6 + HCl) + (TMB + H_2O_2). (C) The corresponding UV-vis absorption spectra of photograph '*B*'. (D) UV-vis absorption spectra of (a) AuNP + (TMB + H_2O_2), (b) ALP + AuNP + HCl + (TMB + H_2O_2), (c) AA-P + AuNP + HCl + (TMB + H_2O_2), and (d) ALP + AA-P + AuNP + HCl + (TMB + H_2O_2) (*Inset*: the corresponding photographs). (E) Calibration curves of (a) the developed enzyme cascade amplification strategy at 650 nm and (b) the conventional enzyme-linked immunosorbent assay at 405 nm toward ALP standards with various concentrations. Error bars indicate standard deviations ($n = 3$).

assay, the carried ALP can trigger the enzyme cascade amplification reaction to produce the colored products. Meanwhile, the absorbance is increased and the visible color is strengthened. By monitoring the change in the absorbance, we can quantitatively determine the concentration of target PSA in the sample. Meanwhile, we can also qualitatively monitor the PSA level by the change in the visible color. In contrast, in the absence of target PSA, the sandwiched immuno-complex can not be formed, thus it can not trigger the progression of enzyme cascade reaction.

Control tests for enzyme cascade amplification strategy (ECAS). To realize our design, one precondition for the signal amplification of ECAS-based colorimetric immunoassay was whether the enzyme cascade reaction could be smoothly progressed in the presence of ALP, as depicted in Fig. 2A. To demonstrate this issue, several control tests were carried out under the different conditions by using the colorimetric measurement (Fig. 2B) and UV-vis absorption spectroscopy (Fig. 2C) (1.0 U mL^{-1} ALP used in this case). As seen from photograph '*c*' in Fig. 2B, almost no color was changed when ALP

and AA-P were mixed together, and the color (i.e., colorless) of the mixture was the same as ALP (photograph 'a') and AA-P (photograph 'b') alone, which was in accordance with the color of the formed AA by the hydrolysis of AA-P. When AuNP, K_2PdCl_6 and HCl were added into the mixture containing ALP and AA-P, significantly, the color of the mixture became gray (photograph 'f') in comparison with pure gold colloids (photograph 'd') and K_2PdCl_6 + HCl (photograph 'e'). Logically, one question arises as to whether PdNS could be successfully formed on the AuNP during this process. To clarify this point, the gray suspension was initially centrifuged and separated, and then the obtained precipitate was monitored by using energy-dispersive X-ray spectroscope (EDX). As seen from Supplementary Fig. S1, palladium and gold elements could be observed in the nanocomposites. Such a result preliminarily indicated that the generated AA by hydrolysis of AA-P could catalyze the formation of PdNS on the surface of AuNP with the aid of ALP.

Furthermore, we also used transmission electron microscope (TEM) to investigate the AuNP before and after reaction with the mixture (Fig. 3). As seen from Fig. 3A, the prepared AuNP was similarly spherical, and the average size was 16 nm. After AuNP was mixed with ALP, AA-P, K_2PdCl_6 and HCl, however, the formed nanoparticles became irregular (Fig. 3B). Moreover, the size of the nanocomposites was obviously larger than that of pure gold nanoparticles. More inspiringly, the UV-vis absorption peak of gold nanoparticles at 518 nm (curve 'd' in Fig. 2C) was disappeared, and no characteristic peaks were observed at the nanocomposites (curve 'f' in Fig. 2C) (Note: The samples were obtained by centrifugation). The results revealed that the surface of AuNP was almost completely coated by the PdNS because of no characteristic absorption peak for the AuNP[40].

As described above, the signal amplification of enzyme cascade reaction mainly derived from the produced PdNS-based peroxidase mimics toward the catalytic oxidation of TMB-H_2O_2 system. As shown photograph 'h' in Fig. 2B, when TMB and H_2O_2 were simultaneously added into the mixture 'f', the color quickly changed from gray to deep blue. Meanwhile, a strong characteristic absorption peak at 650 nm was also achieved (curve 'h' in Fig. 2C). The characteristic peak mainly derived from the catalyzed product of TMB. At the same time, another concern to be produced was whether the enzyme cascade amplification strategy originated from the initial ALP toward the hydrolysis reaction of AA-P. To monitor this issue, another two control tests were implemented in the mixture 'h' in the absence and presence of ALP or AA-P, respectively. As indicated from photographs 'i' and 'j' in Fig. 2B, the visible color in the absence of ALP or AA-P was heavily dimmer than that of photographs 'h'. Moreover, the absorbance values (curves 'i' and 'j' in Fig. 2C) were largely lower than that in the simultaneous presence of ALP and AA-P (curve 'h' in Fig. 2C). To clarify whether the added AuNP alone could cause the development of visible color, gold colloids ($C_{[AuNP]} \approx 1.92$ nM) with various volumes were directly added into 100 μL of substrate solution containing 7.2 M H_2O_2 and 0.5 mM TMB in pH 4.0 sodium citrate-phosphate buffer. As shown from Supplementary Fig. S2, there is little change in the absorbance at 650 nm when the volume of gold colloids was lower than 4 μL (*Note*: 3 μL used in this study), which was in accordance with the observation of Fig. 2D. These results further revealed that (i) the enzyme cascade reaction mainly derived from the hydrolysis reaction of the ALP toward AA-P, (ii) the amplification of detectable signal mainly originated from the product (PdNS) of enzyme cascade reaction, and (iii) the added AuNP could not nearly catalytic oxidation of TMB in the presence of H_2O_2[41].

Kinetic study and mechanism of palladium nanostructures catalytic reactivity. To investigate the catalytic mechanism of the as-prepared PdNS, apparent steady-state kinetic parameters of the catalytic reaction were determined by changing the concentration of TMB and H_2O_2 in this system, respectively (Note: The preparation method of palladium nanostructures was described in the Methods). A series of initial rates were calculated from the absorbance (650 nm, versus time plots) based on the molar absorption coefficient for TMB-derived oxidation products ($\varepsilon_{650nm} = 3.9 \times 10^4$ M^{-1} cm^{-1})[44] by varying one substrate concentration while fixing another substrate concentration. It can be seen that typical Michaelis-Menten curves were obtained for PdNS with both substrates: TMB and H_2O_2 (Fig. 4A–B). To further demonstrate whether the PdNS-based catalytic reaction followed the Michaelis-Menten behavior, Lineweaver-Burk plot was used. As shown in Fig. 4C–D, the reciprocal of initial rate was proportional to the reciprocal of substrate (TMB and H_2O_2) concentration, which was fitted to the double reciprocal of the Michaelis-Menten equation, $1/v = (K_m/V_{max}) \cdot (1/[S]) + 1/V_{max}$, where v is the initial rate, K_m is the Michaelis–Menten constant, V_{max} is the maximum reaction rate, and $[S]$ is the substrate concentration. The results indicated that the reaction followed the Michaelis-Menten behavior. The apparent K_m and V_{max} were obtained using Lineweaver-Burk plot (Supplementary Table S1). As indicated from Table S1, the K_m value of PdNS was higher than that of HRP toward H_2O_2, indicating that the PdNS had a lower affinity toward H_2O_2 than HRP. In contrast, the K_m value was lower than that of HRP toward TMB, indicating that the PdNS had a higher affinity toward TMB than HRP. In addition, the K_{cat} values of PdNS for both TMB ($K_{cat} = 2.09 \times 10^4$ s^{-1}) and H_2O_2 ($K_{cat} = 4.61 \times 10^4$ s^{-1}) were in the midrange of that of the reported nanomaterial-based peroxidase mimics (Supplementary Table S1). These results indicated that PdNS possessed relatively high peroxidase-like activity. The high peroxidase-like activity of PdNS could provide a precondition for realizing ultrasensitive immunoassay based on the ECAS.

To further investigate the catalytic mechanism of PdNS, the catalytic efficiency was evaluated toward TMB and H_2O_2 with various
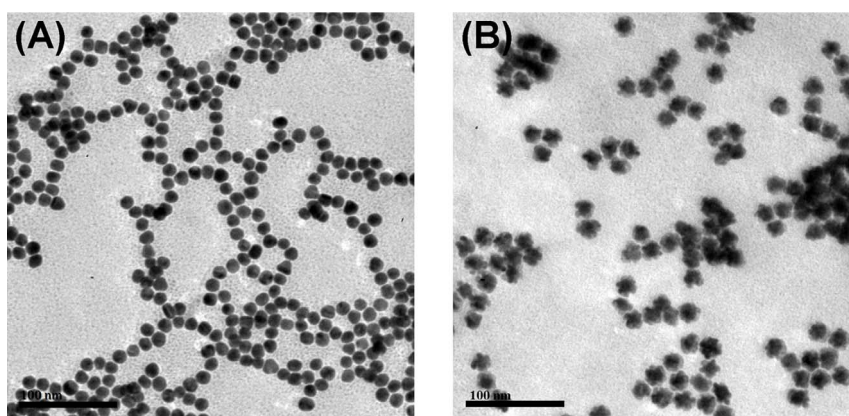
Figure 3 | Typical TEM images of (A) pure gold nanoparticles and (B) PdNS-grown gold nanoparticles after using the enzyme cascade reaction.
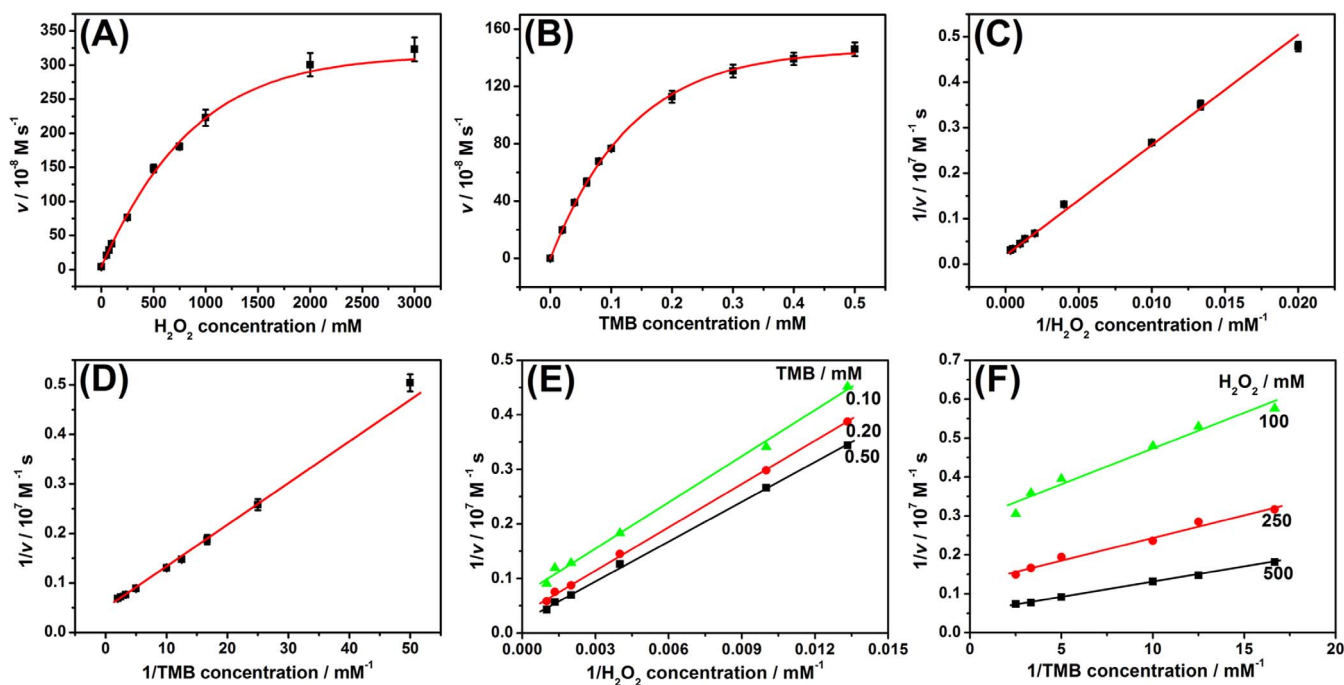
Figure 4 | Steady-state kinetic assay and catalytic characteristics of the palladium nanostructures toward various components: (A,C) 0.5 mM TMB and different-concentration H_2O_2, (B,D) 500 mM H_2O_2 and different-concentration TMB, and (E,F) different-concentration TMB and different-concentration H_2O_2. The initial rate (v) of the reaction was measured using 40 μL of the prepared palladium nanostructures in 400 μL of sodium citrate-phosphate buffer solution (pH 4.0) for 5 min at room temperature. Error bars indicate standard deviations ($n = 3$).

concentrations, respectively. The double reciprocal plots of initial rate versus one substrate concentration were obtained over a range of the secondary substrate concentration (Fig. 4E–F). The slope of the lines is parallel, which is characteristic of a ping-pong mechanism, as is observed for bioactive HRP[43,44] and the reported peroxidase mimics[42,43,45]. The results also indicated that the PdNS were initially bound and reacted with the first substrate, and then released the first product before reaction with the secondary substrate[43]. The released product was hydroxyl radical (•OH) due to the decomposition of H_2O_2 during the catalysis of the PdNS[39,45,46]. The resulting hydroxyl radicals could be stabilized on the surface of the PdNS[47,48], which could react with TMB. Hence, the chemical reaction mechanism of PdNS relative to TMB-H_2O_2 system is schematically illustrated in Supplementary Fig. S3, which was similar with conventional HRP[49] and our previously reported platinum nanostructures[50]. H_2O_2 molecules were initially adsorbed on the surface of PdNS, then activated by the bound palladium to generate the •OH, and then the generated •OH was stabilized on the surface of PdNS. Following that, TMB was oxidized by •OH to form a blue color product.

Optimization of experimental conditions for ECAS. As shown from Fig. 2A, the designed ECAS mainly consisted of the ALP-mediated catalytic hydrolysis of AA-P, the formation of PdNS-based peroxidase mimics and the PdNS-mediated catalytic oxidation of TMB-H_2O_2. In order to acquire an optimal analytical performance, the reaction conditions for ECAS should be optimized. Among these reactions, the catalytic capability of PdNS toward TMB-H_2O_2 system was very crucial since it directly affected the sensitivity of colorimetric immunoassay. Since the generated PdNS was used as peroxidase mimics, we initially investigated the effect of pH of substrate solution, incubation temperature, H_2O_2 concentration and incubation time on the analytical properties of the developed ECAS. As shown from Supplementary Fig. S4, the optimal pH of sodium citrate-phosphate buffer, temperature, H_2O_2 concentration, and incubation time were pH 4.0, 40°C, 7.2 M and 300 s (5 min), respectively. The results were almost in accordance with our previous reports[14,50]. That

is to say, the peroxidase-like activity of nanoparticle-based catalysts is usually much higher in acidic solution than in neutral or basic solutions, and the maximum catalytic efficiency is acquired in the presence of high-concentration H_2O_2. Moreover, we also found that the PdNS-based peroxidase mimics could be successfully generated within a wide pH range of 3.0 to 6.0 (Supplementary Fig. S5).

For the successful development of a highly sensitive ECAS-based colorimetric immunoassay, the low-concentration ALP should be exactly determined by the designed ECAS according to the sandwich-type immunoassay format. To demonstrate the feasibility of the ECAS, two types of assay protocols with and without the enzyme cascade reaction were used for the detection of ALP standards with various concentrations, respectively (Note: During this experimental process, pNPP was used as the substrate of conventional ALP-based amplification strategy while the AA-P with the same-concentration pNPP was utilized for the developed ECAS). The assay protocols for both methods were described detailedly in the Supplementary. As shown in Fig. 2E, the absorbance increased with the increasing ALP concentration for both assay protocols. The detection limit of using the developed ECAS was 0.22 mU mL^{-1} ALP (curve 'a'), whereas that of using the conventional ALP-based amplification strategy was 4.3 mU mL^{-1} ALP (curve 'b'). The results also suggested that the absorbance of using the developed ECAS could be changed only if the concentration of ALP in the sample was higher than 0.22 mU mL^{-1}.

Analytical performance of enhance colorimetric immunoassay using the ECAS. To further demonstrate the capability of the designed ECAS on the colorimetric immunoassay, the as-prepared ALP-Ab$_2$ was used for the detection of target PSA with a sandwich-type immunoassay format in high-binding polypropylene 96-well MTP by coupling with the developed ECAS. Under optimal conditions, PSA standards with various concentrations were monitored in the 96-well MTP by using the designed protocol (Fig. 5B). A sigmoid curve regression between the absorbance and the logarithm of PSA concentration was obtained (curve 'a' in Fig. 5A). The absorbance density increased with the increase of target PSA concentration in
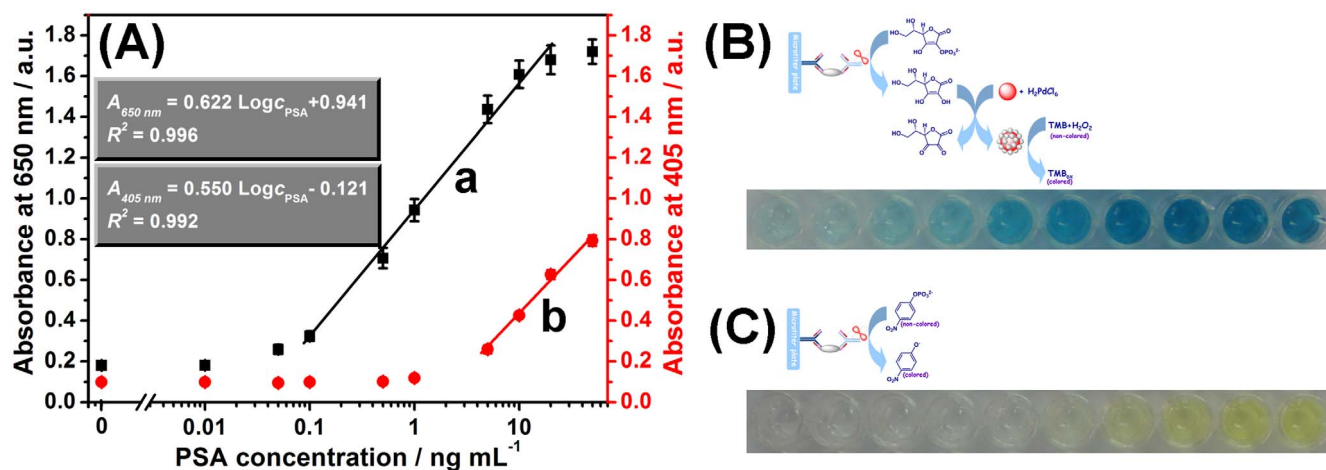
Figure 5 | (A) Calibration plots of various immunoassay protocols toward PSA standards with various concentrations using (a) the developed ECAS-CIA and (b) conventional colorimetric ELISA method, respectively, **(B)** the corresponding photographs of curve '*a*', and **(C)** the corresponding photographs of curve '*b*'. Error bars indicate standard deviations ($n = 8$).

the sample. A linear dependence between the absorbance and the logarithm of PSA level was obtained in the range from 0.1 ng mL^{-1} to 20 ng mL^{-1}. The detection limit (LOD) was 0.05 ng mL^{-1} estimated at a signal-to-noise ration of 3 ($n = 8$). Since the threshold value of total PSA in normal human serum is about 4 ng mL^{-1}, the developed ECAS-CIA can completely meet the requirement of clinical diagnostics. For comparison, we also investigated the analytical properties of the conventional enzyme-labeled colorimetric immunoassay by directly using ALP-labeled Ab$_2$ as detection antibody (Fig. 5C). As shown from curve '*b*' in Fig. 5A, the linear range and LOD by using the conventional ELISA method were 5–50 ng mL^{-1} and 1.0 ng mL^{-1} PSA, respectively. Although the system has not yet been optimized for maximum efficiency, the LOD of the developed ECAS-CIA was close to 10-fold lower than that of commercialized human PSA ELISA kit (LOD: 0.5 ng mL^{-1} PSA, Biocell Biotechnol. Co., Ltd., Zhengzhou, China). The low LOD was mainly ascribed to the enzyme cascade signal amplification efficiency.

The reproducibility and precision of the developed ECAS-CIA were evaluated by calculating the intra- and inter-batch variation coefficients (CVs, $n = 8$). Experimental results indicated that the CVs of the assays using the same-batch immunosensing probes were between 3.5% and 9.5% in all cases (Supplementary Fig. S6 and Table S2). The batch-to-batch reproducibility of the developed ECAS-CIA

was also evaluated by assaying 10 ng mL^{-1} PSA (as an example) for eight times within the different days, and the obtained CV was about 10.7%. The low CVs indicated that the developed ECAS-CIA could be used repeatedly and further revealed the possibility of batch preparation.

To evaluate the specificity of the developed ECAS-CIA for the detection of target PSA, we challenged the system with other interfering substances in human serum, e.g., alpha-fetoprotein (AFP), carcinoembryonic antigen (CEA), cancer antigen 15-3 (CA 15-3), cancer antigen 19-9 (CA 19-9), cancer antigen 125 (CA 125), and human immunoglobulin G (HIgG). The assay was implemented with the same experimental procedures. As shown from Fig. 6A, a significant change in the absorbance density was observed with the target PSA relative to 10-fold higher interfering components. These results revealed that the components coexisting in the sample matrix did not interfere in the determination of PSA, *i.e.*, the developed ECAS-CIA was shown to be sufficiently selective for the detection of target PSA.

Analysis of real samples and evaluation of method accuracy. To monitor the analytical reliability and applicable potential of the developed ECAS-CIA for testing real samples, we collected 36 human serum specimens with various PSA levels from Fujian Provincial Hospital of China according to the rules of the local ethical
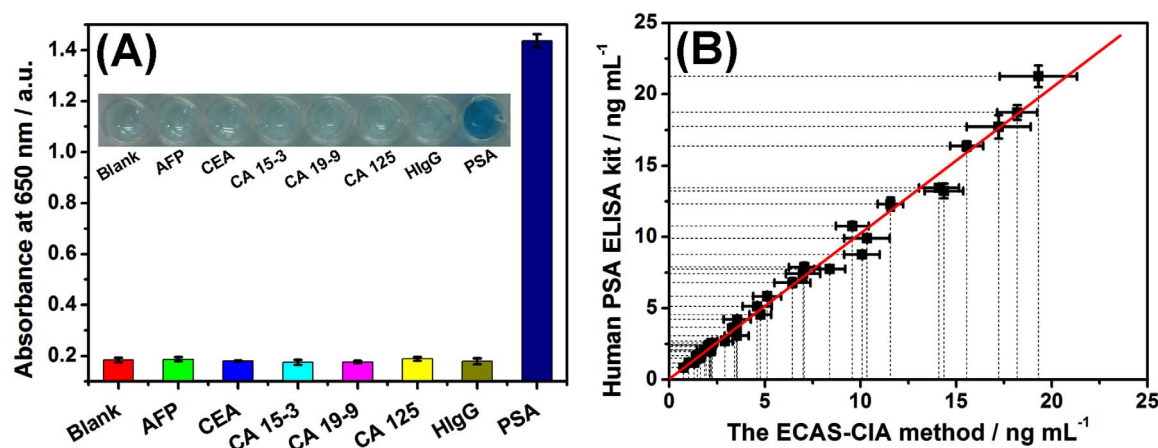
Figure 6 | (A) The specificity of the developed ECAS-CIA toward PSA (5 ng mL^{-1}), AFP (50 ng mL^{-1}), CEA (50 ng mL^{-1}), CA 15-3 (50 U mL^{-1}), CA 19-9 (50 U mL^{-1}), CA 125 (50 U mL^{-1}) and HIgG (50 ng mL^{-1}) (*Inset*: the corresponding photographs), and **(B)** comparison of the assay results toward PSA clinical serum specimens by using the developed ECAS-CIA and commercialized human PSA ELISA kit, respectively. Error bars indicate standard deviations ($n = 3$).

committee. Prior to measurement, these samples were gently shaken at RT (Note: all handling and processing were performed carefully, and all tools in contact with patient specimens and immunoreagents were disinfected after use), and then evaluated by using the developed ECAS-CIA. The assayed results were compared with those obtained by using the commercially available human PSA ELISA kit (Biocell Biotechnol. Co., Ltd., Zhengzhou, China). The results are listed in Table S3. Statistical analysis of the experimental results was performed using a t-test and linear regression analysis between two methods. As seen from Table S3, the t_{exp} values in all samples were less than t_{crit} ($t_{crit [4, 0.05]} = 2.77$). The regression line was fitted to $y = 1.020x + 0.052$ ($R^2 = 0.994, n = 102$) where x stands for the PSA concentrations estimated with the developed immunoassay and y stands for those of the reference procedure (Fig. 6B), indicating that the results obtained from these two methods matched within the experimental error. Importantly, two low-concentration PSA samples were estimated as negative. Because of sample dilution, two samples as negatives determined by the commercialized human PSA ELISA kit were detected with the concentrations of 0.167 and 0.462 ng mL^{-1}, respectively. Hence, the developed ECAS-CIA could be regarded as an optional scheme for sensitive monitoring of target PSA with high accuracy.

Discussion

In summary, we for the first time demonstrate the ability of an enhanced colorimetric immunoassay for highly sensitive detection of low-abundance proteins (PSA used as a model) in biological fluids by using single enzyme-catalyzed cascade signal amplification strategy. As described above, the designed enzyme cascade amplification strategy could be smoothly progressed in the presence of ALP. The formed palladium nanocatalyst possessed high peroxidase-like activity with a typical Michaelis-Menten kinetics. Differentiated from conventional enzyme-linked colorimetric immunoassay, the detectable signal does not originated from the labeled enzyme, but from the product (i.e., PdNS-based peroxidase mimics) of enzyme cascade reaction. In this case, the background signal reduction and the detectable signal amplification can be successfully achieved. Compared with nanostructure-based signal amplification strategy, the ECAS-CIA can efficiently maintain the orientation of detection antibody in the soluble phase, decrease the steric-hindrance of the labeled antibody on the nanoparticles, and avoid the non-specific adsorption of nanoparticles toward target proteins. Despite the participation of nanoparticles in this work, the PdNS-based peroxidase mimics, can be only produced by the labeled ALP on the detection antibody in the presence of target analyte. The presence of AuNP is only used as the seeds for the growth of PdNS, and it does not exhibit the catalytic capacity toward TMB-H$_2$O$_2$. In addition, the methodology can avoid the multiple labels and use of multiple enzymes. Highlight of this work is to adequately utilize high catalytic efficiency of ALP and the high peroxidase-like activity of PdNS relative to TMB-H$_2$O$_2$ system. More impressively, the developed ECAS-CIA method does not require sophisticated instruments, and is well suitable for high-throughput biomedical sensing and application in the clinical automatic immunoassay analyzer, even possible to realize the commercialization. Future work should be focused on other low-abundance proteins by controlling the target antibody, thereby demonstrating the versatility of the assay scheme.

Methods

Reagents and chemicals. Mouse monoclonal anti-human PSA antibody (designated as Ab$_1$) was purchased from Abcam (Cambridge, MA). Goat polyclonal anti-human PSA antibody (designated as Ab$_2$) was achieved from ImmunoReagents, Inc. (Raleigh, NC). PSA standards were obtained from Biocell Biotechnol. Co., Ltd (Zhengzhou, China). Alkaline phosphatase (ALP, from calf intestine) was purchased from Toyobo (Osaka, Japan). 4-Nitrophenyl phosphate disodium salt hexahydrate (pNPP) was from Alfa Aesar (Tianjin, China). L-Ascorbic acid 2-phosphate sesquimagnesium salt hydrate (AA-P) was purchased from Sigma-Aldrich (St. Louis, MO). 3,3′,5,5′-Tetramethylbenzidine (TMB) and bovine serum albumin (BSA) were

acquired from Sinopharm Chem. Re. Co., Ltd (Shanghai, China). Potassium hexachloropalladate (K$_2$PdCl$_6$) and diethanolamine (DEA) were obtained from Aladdin (Shanghai, China). High-binding polystyrene 96-well microtiter plates were obtained from Greiner Bio-One (Frickenhausen, Germany, cat#: 655061). Gold colloids (AuNP) with 16 nm in diameter were prepared and characterized as described[51]. All other reagents were of analytical grade and were used without further purification. Ultrapure water was obtained from a Millipore water purification system (18 MΩ, Milli-Q, Millipore) was used in all runs. Clinical serum samples were made available by Fujian Provincial Hospital, China.

A pH 9.6 carbonate buffer (1.69 g Na$_2$CO$_3$ and 2.86 g NaHCO$_3$), a pH 9.8 carbonate buffer (2.33 g Na$_2$CO$_3$ and 2.35 g NaHCO$_3$), and a pH 7.4 phosphate-buffered saline (PBS, 0.01 M) (2.9 g Na$_2$HPO$_4$·12H$_2$O, 0.24 g KH$_2$PO$_4$, 0.2 g KCl and 8.0 g NaCl) were prepared by adding the corresponding chemicals in 1000-mL distilled water, respectively. The blocking buffer and washing buffer were obtained by adding 1.0 wt % BSA and 0.05% Tween 20 (v/v) in PBS, respectively.

Preparation of ALP-Ab$_2$ conjugates (ALP-Ab$_2$). ALP-labeled polyclonal goat anti-human PSA antibody (ALP-Ab$_2$) was prepared by using an alkaline phosphatase labeling kit-NH$_2$ (Dojindo China Co., Ltd. Shanghai, China), and the labeling process was described in detail in the general information of this kit. NH$_2$-reactive ALP (a component of this kit) has activated ester groups, and can easily make a covalent bond with an amino group of the target molecule without any activation process. Briefly, 1-mL washing buffer and 0.5-mL Ab$_2$ (1.0 mg mL^{-1}) were initially injected into the filtration tube and centrifuged at 7000 g for 30 min. Then 1-mL reaction buffer was added into the filtration tube and centrifuged once more. Meanwhile, 50-μL reaction buffer was added into the NH$_2$-reactive ALP and dissolved with pipetting. Following that, the NH$_2$-reactive ALP solution was dropped into the Ab$_2$ solution, which was concentrated to about 50 μL. After pipetting several times, the mixture was incubated for 2 h at 37°C. Afterward, 1.9-mL storage buffer was added into the mixture, and pipetted for 10 times to recover the conjugate. Finally, the formed ALP-Ab$_2$ conjugates were transferred to a microtube and stored at 4°C for further use.

Enhanced colorimetric immunoassay protocol using enzyme cascade amplification strategy (ECAS-CIA). Fig. 1 displays the measurement protocol of ECAS-CIA. A high-binding polystyrene 96-well microtiter plate (MTP) was coated overnight at 4°C with 50 μL per well of Ab$_1$ at a concentration of 10 μg mL^{-1} in 0.05 M sodium carbonate buffer (pH 9.6). The MTP was covered with adhesive plastics plate sealing film to prevent evaporation. On the following day, the MTP was washed three times with washing buffer, and then incubated with 300 μL per well of blocking buffer for 1 h at 37°C with shaking. The MTP was then washed as before. Following that, 50 μL of PSA standards or samples with various concentrations was added into the MTP, and incubated for 1 h at 37°C under shaking. After washing, 50 μL of the ALP-Ab$_2$ solution was added into the well and incubated for 1 h at 37°C with shaking. The plates were washed three times with washing buffer and one time with water, and then 20 μL of substrate solution containing 5.0 mM AA-P and 1.0 mM MgCl$_2$ in carbonate buffer (pH 9.8) was added to each well and incubated at 37°C for 20 min. Subsequently, 3-μL gold colloids (C$_{[AuNP]}$ ≈ 1.92 nM), 1.5-μL HCl solution (1.0 M), and 2-μL K$_2$PdCl$_6$ solution (1.5 mM) were simultaneously added to the resultant solution and incubated at 37°C for 5 min. After that, 100 μL of substrate solution containing 7.2 M H$_2$O$_2$ and 0.5 mM TMB in pH 4.0 sodium citrate-phosphate buffer was added and incubated at 40°C for 5 min for color development. Meanwhile, the absorbance was read at 650 nm with a plate reader (DNM-9602, Beijing Perlong Medical Instrument Ltd, China). For comparison, traditional ALP-based ELISA method was also used for the detection of PSA in the substrate solution including 5.0 mM pNPP and 1.0-mM MgCl$_2$ in 10% DEA buffer (pH 9.8) with the same assay format after shaking the MTP for 30 min at 37°C. All measurements were conducted at room temperature (25 ± 1.0°C). Analyses are always made in triplicate. The reactions between two methods were not stopped with stop buffer in order to facilitate comparison.

1. Zhu, C. et al. Single-layer MoS$_2$-based nanoprobes for homogeneous detection of biomolecules. *J. Am. Chem. Soc.* **135**, 5998–6001 (2013).
2. de la Rica, R. & Stevens, M. M. Plasmonic ELISA for the ultrasensitive detection of disease biomarkers with the naked eye. *Nat. Nanotechnol.* **7**, 821–824 (2012).
3. Rodríguez-Lorenzo, L., de la Rica, R., Álvarez-Puebla, R. A., Liz-Marzán, L. M. & Stevens, M. M. Plasmonic nanosensors with inverse sensitivity bymeans of enzyme-guided crystal growth. *Nat. Mater.* **11**, 604–607 (2012).
4. Rusling, J. F. Multiplexed electrochemical protein detection and translation to personalized cancer diagnostics. *Anal. Chem.* **85**, 5304–5310 (2013).
5. Gubala, V., Harris, L. F., Ricco, A. J., Tan, M. X. & Williams, D. E. Point of care diagnostics: status and future. *Anal. Chem.* **84**, 487–515 (2012).
6. Aragay, G., Pino, F. & Merkoci, A. Nanomaterials for sensing and destroying pesticides. *Chem. Rev.* **112**, 5317–5338 (2012).
7. Perfezou, M., Turner, A. & Merkoci, A. Cancer detection using nanoparticle-based sensors. *Chem. Soc. Rev.* **41**, 2606–2622 (2012).
8. Krishnan, S., Mani, V., Wasalathanthri, D., Kumar, C. V. & Rusling, J. F. Attomolar detection of a cancer biomarker protein in serum by surface plasmon resonance using superparamagnetic particle labels. *Angew. Chem., Int. Ed.* **50**, 1175–1178 (2011).

9. Tang, D., Zhang, B., Tang, J., Hou, L., & Chen, G. Displacement-type quartz crystal microbalance immunosensing platform for ultrasensitive monitoring of small molecular toxins. *Anal. Chem.* **85**, 6958–6966 (2013).

10. Yuan, L., Xu, L. & Liu, S. Integrated tyramide and polymerization-assisted signal amplification for a highly-sensitive immunoassay. *Anal. Chem.* **84**, 10737–10744 (2012).

11. Geißler, D., Stufler, S., Löhmannsröben, H. G. & Hildebrandt, N. Six-color time-resolved förster resonance energy transfer for ultrasensitive multiplexed biosensing. *J. Am. Chem. Soc.* **135**, 1102–1109 (2013).

12. Akhavan-Tafti, H. *et al.* A homogeneous chemiluminescent immunoassay method. *J. Am. Chem. Soc.* **135**, 4191–4194 (2013).

13. Munge, B. S. *et al.* Nanostructured immunosensor for attomolar detection of cancer biomarker interleukin-8 using massively labeled superparamagnetic particles. *Angew. Chem., Int. Ed.* **50**, 7915–7918 (2011).

14. Gao, Z., Xu, M., Hou, L., Chen, G. & Tang, D. Magnetic bead-based reverse colorimetric immunoassay strategy for sensing biomolecules. *Anal. Chem.* **85**, 6945–6952 (2013).

15. Malashikhina, N., Garai-Ibabe, G. & Pavlov, V. Unconventional application of conventional enzymatic substrate: first fluorogenic immunoassay based on enzymatic formation of quantum dots. *Anal. Chem.* **85**, 6866–6870 (2013).

16. Wu, Y., Liu, S. & He, L. Electrochemical biosensing using amplification-by-polymerization. *Anal. Chem.* **81**, 7015–7021 (2009).

17. Lin, H. *et al.* Modified enzyme-linked immunosorbent assay strategy using graphene oxide sheets and gold nanoparticles functionalized with different antibody types. *Anal. Chem.* **85**, 6228–6232 (2013).

18. Jiang, W. *et al.* Simultaneous determination of 13 fluoroquinolone and 22 sulfonamide residues in milk by a dual-colorimetric enzyme-linked immunosorbent assay. *Anal. Chem.* **85**, 1995–1999 (2013).

19. Deshpande, S. S. *Enzyme Immunoassays: From Concept to Product Development.* (Kluwer Academic Publishers, Dordrecht; 1996).

20. Obzansky, D. M. Sensitive, colorimetric enzyme amplification cascade for determination of alkaline phosphatase and application of the method to an immunoassay of thyrotropin. *Clin. Chem.* **37**, 1513–1518 (1991).

21. Liu, Q. & Boyd, B. J. Liposomes in biosensors. *Analyst* **138**, 391–409 (2013).

22. Ambrosi, A., Airo, F. & Merkoci, A. Enhanced gold nanoparticle based ELISA for a breast cancer biomarker. *Anal. Chem.* **82**, 1151–1156 (2010).

23. Zhang, Q. *et al.* Nanotube-based colorimetric probe for ultrasensitive detection of ataxia telangiectasia mutated protein. *Anal. Chem.* **83**, 9191–9196 (2011).

24. Kanno, S., Yanagida, Y., Haruyama, T., Kobatake, E. & Aizawa, M. Assembling of engineered IgG-binding protein on gold surface for highly oriented antibody immobilization. *J. Biotechnol.* **76**, 207–214 (2000).

25. Tang, D. Niessner, R. & Knopp, D. Flow-injection electrochemical immunosensor for the detection of human IgG based on glucose oxidase-derivated biomimetic interface. *Biosens. Bioelectron.* **24**, 2125–2130 (2009).

26. Zhang, H. & Meyerhoff, M. E. Gold-coated magnetic particles for solid-phase immunoassays: enhancing immobilized antibody binding efficiency and analytical performance. *Anal. Chem.* **78**, 609–616 (2006).

27. Zhang, H., Li, F., Dever, B., Li, X. & Le, X. C. DNA-mediated homogeneous binding assays for nucleic acids and proteins. *Chem. Rev.* **113**, 2812–2841 (2013).

28. Liu, M., Zhao, H., Chen, S., Yu, H. & Quan, X. Interface engineering catalytic graphene for smart colorimetric biosensing. *ACS Nano* **6**, 3142–3151 (2012).

29. Zhang, B. *et al.* DNA-based hybridization chain reaction for amplified bioelectronic signal and ultrasensitive detection of proteins. *Anal. Chem.* **84**, 5392–5399 (2012).

30. Zhou, P. Immunoassays with protein misfolding cycle amplification: a platform for ultrasensitive detection of antigen. *Anal. Chem.* **84**, 7343–7349 (2012).

31. Lehninger, A. L., Nelson, D. L. & Cox, M. M. *Lehninger Principles of Biochemistry* 5th edn. (W. H. Freeman, New York; 2008).

32. Zauner, T., Berger-Hoffmann, R., Muller, K., Hoffmann, R. & Zuchner, T. Highly adaptable and sensitive protease assay based on fluorescence resonance energy transfer. *Anal. Chem.* **83**, 7356–7363 (2011).

33. Uludag, Y. & Tothill, I. E. Cancer biomarker detection in serum samples using surface plasmon resonance and quartz crystal microbalance sensors with nanoparticle signal amplification. *Anal. Chem.* **84**, 5898–5904 (2012).

34. Akter, R., Rahman, M. A. & Rhee, C. K. Amplified electrochemical detection of a cancer biomarker by enhanced precipitation using horseradish peroxidase attached on carbon nanotubes. *Anal. Chem.* **84**, 6407–6415 (2012).

35. Catalona, W. J. *et al.* Comparison of digital rectal examination and serum prostate specific antigen in the early detection of prostate cancer: results of a multicenter clinical trial of 6,630 men. *J. Urol.* **151**, 1283–1290 (1994).

36. Zhao, W., Ma, Z., Yan, D., Xu, J. & Chen, H. In situ enzymatic ascorbic acid production as electron donor for CdS quantum dots equipped TiO₂ nanotubes: a general and efficient approach for new photoelectrochemical immunoassay. *Anal. Chem.* **84**, 10518–10521 (2012).

37. Chen, H. *et al.* Plasmonic percolation: plasmon-manifested dielectric-to-metal transition. *ACS Nano* **6**, 7162–7171 (2012).

38. Kim, J., Chung, H. & Lee, T. R. Preparation and characterization of palladium shells with gold and silica cores. *Chem. Mater.* **18**, 4115–4120 (2006).

39. He, W. *et al.* Design of AgM bimetallic alloy nanostructures (M= Au, Pd, Pt) with tunable morphology and peroxidase-like activity. *Chem. Mater.* **22**, 2988–2994 (2010).

40. Kim, J. *et al.* Gold, palladium, and gold−palladium alloy nanoshells on silica nanoparticle cores. *ACS Appl. Mater. Interfaces* **1**, 1063–1069 (2009).

41. Jv, Y., Li, B. & Cao, R. Positively-charged gold nanoparticles as peroxidase mimic and their application in hydrogen peroxide and glucose detection. *Chem. Commun.* **46**, 8017–8019 (2010).

42. Zhang, X. *et al.* Prussian blue modified iron oxide magnetic nanoparticles and their high peroxidase-like activity. *J. Mater. Chem.* **20**, 5110–5116 (2010).

43. Gao, L. *et al.* Intrinsic peroxidase-like activity of ferromagnetic nanoparticles. *Nat. Nanotechnol.* **2**, 577–583 (2007).

44. Proter, D. & Bright, H. The mechanism of oxidation of nitroalkanes by horseradish peroxidase. *J. Biolog. Chem.* **258**, 9913–9924 (1982).

45. Su, L. *et al.* Colorimetric detection of urine glucose based ZnFe₂O₄ magnetic nanoparticles. *Anal. Chem.* **84**, 5753–5758 (2012).

46. Ge, S. *et al.* Colorimetric assay of K-562 cells based folic acid-conjugated porous bimetallic Pd@Au nanoparticles for point-of-care testing. *Chem. Commun.* **50**, 475–477 (2014).

47. Zhang, Z., Berg, A., Levanon, H., Fessenden, R. & Meisel, D. On the interactions of free radicals with gold nanoparticles. *J. Am. Chem. Soc.* **125**, 7959–7963 (2003).

48. Yuan, S., Chen, M., Mao, X. & Alshawabkeh, A. N. Effects of reduced sulfur compounds on Pd-catalytic hydrodechlorination of trichloroethylene in groundwater by cathodic H₂ under electrochemically induced oxidizing conditions. *Environ. Sci. Technol.* **47**, 10502–10509 (2013).

49. Frey, A., Mechelein, B., Externest, D. & Schmidt, M. A stable and highly sensitive 3, 3′, 5, 5′-tetramethylbenzidine-based substrate reagent for enzyme-linked immunosorbent assays. *J. Immunol. Methods* **233**, 47–56 (2000).

50. Gao, Z., Xu, M., Hou, L., Chen, G. & Tang, D. Irregular-shaped platinum nanoparticles as peroxidase mimics for highly efficient colorimetric immunoassay. *Anal. Chim. Acta* **776**, 79–86 (2013).

51. Yuan, R. *et al.* Ultrasensitive potentiometric immunosensor based on SA and OCA techniques for immobilization of HBsAb with colloidal Au and polyvinyl butyral as matrixes. *Langmuir* **20**, 7240–7245 (2004).

Acknowledgments

Author contributions

D.T. supervised and directed the overall project. Z.G. and D.T. conceived and designed the experiments and wrote the main manuscript text. Z.G., L.H. and M.X. performed experiments. All authors contributed to the data analysis and reviewed the manuscript.

Additional information